Q. J. R. Meteorol. Soc. (2006), **132**, pp. 1259–1281 doi: 10.1256/qj.05.153

Multiple-scattering microwave radiative transfer for data assimilation applications

By PETER BAUER[1]*, EMMANUEL MOREAU[2], FRÉDÉRIC CHEVALLIER[3] and UNA O'KEEFFE[4]

[1]*European Centre for Medium-Range Weather Forecasts, UK*
[2]*NOVIMET, France*
[3]*Laboratoire des Sciences du Climat et l'Environnement, France*
[4]*The Met Office, UK*

(Received 22 June 2005; revised 28 December 2005)

SUMMARY

A multiple-scattering radiative transfer model for microwave radiance data assimilation in global numerical weather-prediction models is presented. The model is part of the RTTOV software package and includes forward, tangent-linear, adjoint and Jacobian models. The model is based on the Eddington approximation to radiative transfer which produces mean errors of less than 0.5 K at the targeted microwave frequencies between 10 and 200 GHz. The simplified treatment of subgrid-scale cloud cover may produce biased model calculations that show a maximum at 0.5 cloud cover and may reach several degrees K. These errors may be corrected with a simple bias correction. Linearity tests indicate that, given a screening procedure that excludes situations in which the model responds nonlinearly to input perturbations, channels near 50.3, 19.35, 22.235 and 183.31 GHz may be used in global radiance data assimilation.

KEYWORDS: Clouds and precipitation Microwave radiance transfer Numerical weather prediction

1. INTRODUCTION

In recent years, the potential assimilation of information from clouds and precipitation has arisen from increased spatial resolution of global numerical weather-prediction (NWP) models and better moist physical parametrizations that produce hydrometeor distributions through large-scale condensation and convection. The choice of observational data depends upon the scale of the application and the observational update cycle as well as the sensitivity of the observations to the moist physical process models. For smaller scales and rapid model cycling within shorter assimilation windows, geostationary observations may be favourable even though the available visible/infrared observations have little sensitivity to atmospheric layers below cloud top. Based on adjoint sensitivity studies, Greenwald *et al.* (2004) could show that even narrow sensitivity profiles of visible/infrared radiances to cloud optical property perturbations offer some potential for constraining cloud prediction (see also Vukićević *et al.* 2004). For larger-scale modelling systems with longer assimilation windows (say 6–12 hours), microwave observations from low orbiting satellites may be favourable because they contain more information on lower cloud and precipitation layers (e.g. Chevallier *et al.* 2002).

Apart from the moist physical parametrizations, modelling of the radiative transfer is part of the observation operator that is required for methods of this type. The model must be accurate and computationally efficient at the same time. Since the explicit treatment of multiple scattering in models that resolve the angular dependence of radiation propagation is too time consuming, only approximative methods are applicable. Greenwald *et al.* (2002) developed such a radiative transfer model for the modelling of visible/infrared radiances as observed from the Geostationary Operational Environmental Satellite (GOES) system in cloudy conditions. While the probability distribution of simulated radiances matched observations rather well, significant deviations were

* Corresponding author: ECMWF, Shinfield Park, Reading RG2 9AX, UK.
e-mail: Peter.Bauer@ecmwf.int

produced depending on cloud evolution stage. These deviations are the combined effect of shortcomings in cloud and radiative transfer modelling. This also indicates a potential for cloudy radiance assimilation if these deviations are not excessive and observation and modelling errors are properly accounted for in the data assimilation system.

Centimetre and millimetre wavelengths penetrate most clouds and exhibit sensitivity to liquid and frozen precipitation. Depending on the choice of frequencies and radiation polarization, cloud and precipitation profile properties may be inferred in most meteorological situations. Microwave observations therefore offer the largest potential for constraining model analyses in the presence of diabatic processes. Since the 1970s, Eddington's second approximation to radiative transfer has been applied to microwave radiative transfer modelling in clouds and precipitation (e.g. Weinman and Davies 1978) for one-dimensional and three-dimensional problems. In most applications and for frequencies below 200 GHz, the modelling errors were found to be well below the signal variability from surface emissivity as well as cloud and precipitation contributions (Kummerow 1993; Smith *et al.* 2002). These studies also recommend the inclusion of the so-called 'delta-scaling' of the optical parameters that accounts for the highly asymmetric phase function in the presence of strongly scattering atmospheres (Joseph *et al.* 1976). Radiative transfer modelling errors below 1 K were obtained for various surface types and observation angles (Smith *et al.* 2002).

At the European Centre for Medium-Range Weather Forecasts (ECMWF), the modelling of Special Sensor Microwave/Imager (SSM/I) brightness temperatures (TBs) from global model fields has been tested (Chevallier and Bauer 2003) and encouraged the utilization of radiances in a one-dimensional variational retrieval (1D-Var) of temperature and humidity in precipitation (Moreau *et al.* 2003). The results indicated that the assimilation of rain-affected microwave radiances is feasible and may constrain NWP analyses in otherwise data void areas. Further developments have led to the operational implementation of a combined 1D+4D-Var assimilation method of SSM/I radiances in clouds and precipitation at ECMWF (Bauer *et al.* 2006a,b).

The successful implementation of the Delta-Eddington model in the data assimilation system at ECMWF has led to its inclusion in the 'Radiative Transfer model for TIROS Operational Vertical Sounder' (RTTOV) (Eyre 1991; Saunders *et al.* 2005) since RTTOV version 8. Since RTTOV aims at applications in NWP, the code is designed for optimal computational efficiency and by making available the forward, tangent-linear, adjoint and k-versions of the code. The k-version refers to the code that can be used for calculating the model Jacobian matrices that contain the partial derivatives of TBs due to perturbations in input parameters.

This paper shortly introduces the technical implementation of the Delta-Eddington approximation and presents extensive testing of forward and tangent-linear model versions. All results were produced for passive microwave channels available from the Special Sensor Microwave Imager Sounder (SSMIS), e.g. Swadley and Chandler (1992). This instrument was launched on 15 October 2003, on board the F-16 platform of the Defense Meteorological Satellite Program maintained by the US Navy. The SSMIS was chosen because it comprises the observational capabilities of a microwave imager with channels that are located in spectral windows with those of a temperature and humidity sounder. Table 1 summarizes the basic channel specifications. Most channels have either single or dual polarization while those denoted with 'rc' have right-hand circular polarizations. These are simulated as the average between vertically and horizontally polarized TBs in RTTOV. Channels 19–24 are new channels that provide temperature soundings of the mesosphere and that are of little importance for radiative transfer applications to tropospheric clouds and precipitation.

TABLE 1. BASIC SSMIS CHANNEL CHARACTERISTICS

Channel	Centre ± 1st ± 2nd sideband frequency (GHz)	Polarization	ΔTB_C at $C = 0.5$ (K)
1	50.3	v	1.03
2	52.8	v	0.03
3	53.596	v	0.04
4	54.4	v	0.04
5	55.5	v	0.01
6	57.29	rc	0.01
7	59.4	rc	0.01
8	150.0 ± 1.25	h	1.25
9	183.31 ± 6.6	h	0.03
10	183.31 ± 3.0	h	0.04
11	183.31 ± 1.0	h	0.05
12	19.35	h	2.17
13	19.35	v	1.20
14	22.235	v	1.11
15	37.0	h	5.16
16	37.0	v	2.61
17	91.655	v	1.65
18	91.655	h	4.77
19	63.283 ± 0.285	rc	0.09
20	60.792 ± 0.358	rc	0.13
21	60.792 ± 0.358 ± 0.002	rc	0.09
22	60.792 ± 0.358 ± 0.006	rc	0.01
23	60.792 ± 0.358 ± 0.016	rc	0.01
24	60.792 ± 0.358 ± 0.05	rc	0.01

TB is brightness temperature and C fractional cloud cover; 'v','h' and 'rc' are vertical, horizontal and right circular polarization, respectively.

Section 2 briefly introduces some model definitions, the appendix outlines the model implementation, while section 3 presents the model evaluation. The paper concludes with an outlook on future developments and perspectives of radiance data assimilation in NWP. The entire model code is available to the NWP community through the NWP Satellite Application Facility (NWP-SAF) (find under www.metoffice.gov.uk). The RTTOV model that accounts for multiple scattering at microwave frequencies is denoted RTTOV-SCATT hereafter.

2. MODEL

In data assimilation, the general forward and inverse problems are formulated using simulated observation vector $\mathbf{y}$ (here TBs) and state vector $\mathbf{x}$. For RTTOV-SCATT, $\mathbf{x}$ contains profiles of pressure p, temperature T, specific humidity q, cloud liquid-water w_{L} and ice w_{I} mixing ratios, rain w_{R} and snow w_{S} fluxes, fractional cloud cover C as well as a number of surface variables required for surface emission and reflection calculations. The input and output parameters are summarized in Table 2. The forward model is

$$\mathbf{y} = H(\mathbf{x}) + \epsilon, \tag{1}$$

with H being the (nonlinear) radiative transfer model and ϵ being the modelling error. In variational data assimilation, also the tangent-linear $\mathbf{H}$,

$$\delta\mathbf{y} = \mathbf{H}\delta\mathbf{x}, \tag{2}$$

and the adjoint $\mathbf{H}^{\mathrm{T}}$ operators are required for the minimization of the cost function whose gradient quantifies the proximity to the optimum solution (for formal details

TABLE 2. RTTOV-SCATT INPUT PARAMETERS

Parameter	Unit	Dimension
Pressure	hPa	RT/ML
Temperature	K	RT/ML
Specific humidity	ppmv	RT/ML
Cloud cover		ML
Cloud liquid-water mixing ratio	kg kg^{-1}	ML
Cloud ice mixing ratio	kg kg^{-1}	ML
Rain flux	kg m^{-2}s^{-1}	ML
Snow flux	kg m^{-2}s^{-1}	ML
Surface pressure	hPa	1
2 m specific humidity	ppmv	1
2 m temperature	K	1
10 m windspeed u-component	m s^{-1}	1
10 m windspeed v-component	m s^{-1}	1
Surface skin temperature	K	1
Zenith angle	degrees	1
Surface type		1
Surface emissivity		1

Parameters with both model level ML and RTTOV-level RT dimensions are used in both RTTOV-SCATT and clear-sky RTTOV routines, respectively. Negative preset surface emissivities activate FASTEM-2 sea surface emissivity model (Deblonde and English 2001).

refer to, e.g. Ide *et al.* 1997). The tangent-linear model produces the perturbation of $\mathbf{y}$, $\delta\mathbf{y}$, at state $\mathbf{x}$ for given perturbations in $\mathbf{x}$, namely $\delta\mathbf{x}$. The k-model produces the Jacobian matrix that is the derivatives of all elements of $\mathbf{y}$ to perturbations of all elements of $\mathbf{x}$. Here, it is calculated as the perturbation in $\mathbf{x}$ that produces a 1 K perturbation in $\mathbf{y}$. The adjoint model is used to compute the transpose of the Jacobian matrix. This Jacobian matrix is usually used to produce the gradient of a cost function with respect to a state vector given the sensitivity of the observations to changes in the state vector. Adjoint models are very efficient computational tools (they avoid the need for perturbation methods and heavy storage burden in Jacobian calculations) used in optimization problems with large state vectors and a crucial ingredient in most operational variational data assimilation systems.

All tests have been performed with a model profile dataset that was produced by the ECMWF 1D+4D-Var rain assimilation system (Bauer *et al.* 2006a,b). The dataset consists of 8290 profiles that are located in tropical areas on 31 December 2004, and that were used in the 00 UTC ECMWF analysis. The profiles are representative for a horizontal resolution of about 40 km. A tropical dataset was chosen to ensure the presence of deep clouds and intense precipitation so that multiple scattering is maximized. Figure 1 shows mean and mean plus/minus one standard deviation of T, q, w_{L}, w_{I}, w_{R}, w_{S} and C, respectively. The distributions cover a significant range of variability. The y-axes refer to model levels that are adjusted according to surface pressure (at model level 60), for example levels 20, 30, 40, 50 and 60 correspond to 40, 215, 560, 900 and 1013 hPa. All simulations are performed over an ocean surface given the local sea surface temperature and near-surface wind speed.

3. MODEL EVALUATION

The following evaluation investigates several aspects that are crucial for the usage of RTTOV-SCATT in data assimilation and general forward modelling. For an illustration of the SSMIS channel's sensitivity to clear and cloudy atmospheric variables,

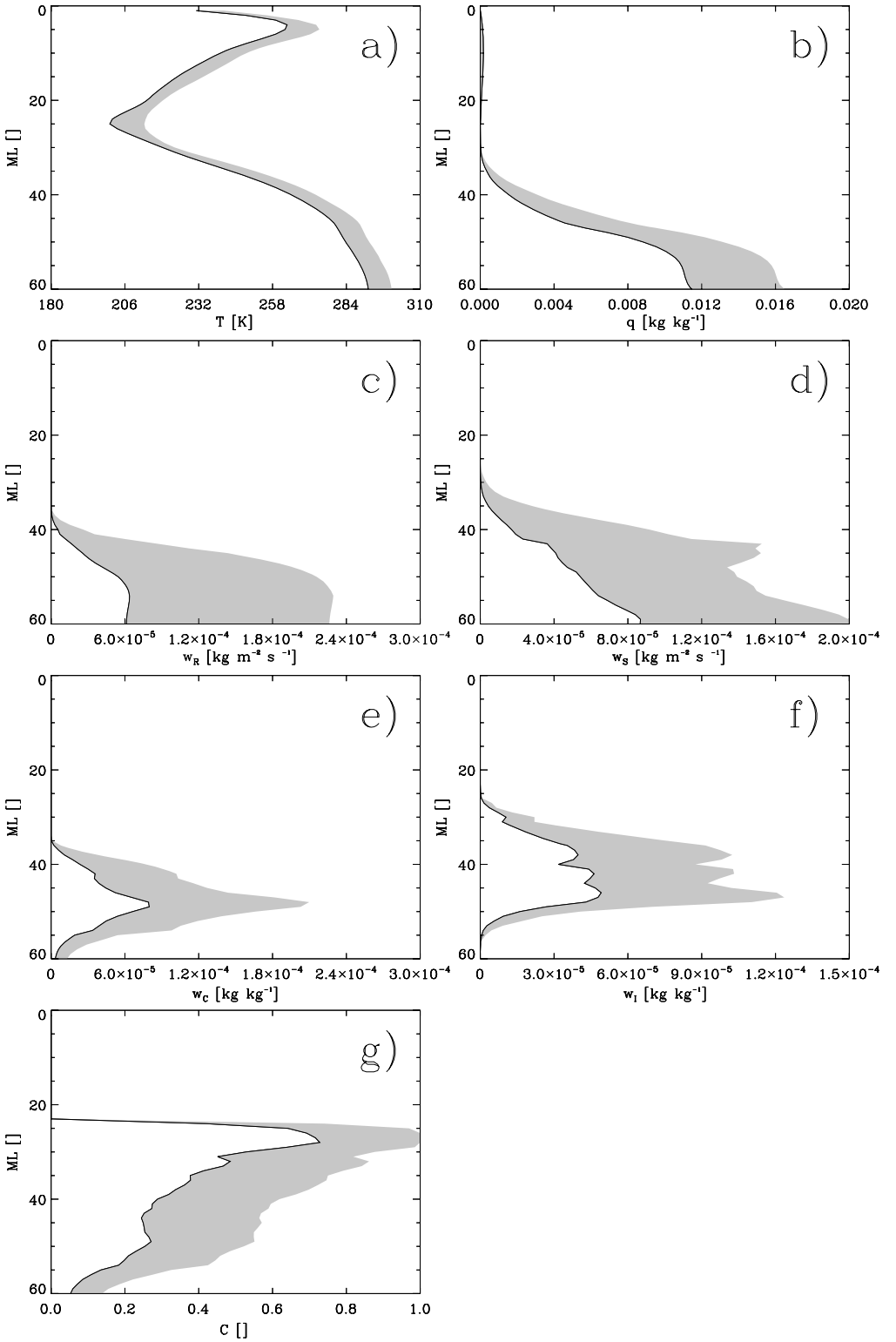

Figure 1. Mean (solid line) and mean+1 standard deviation of (a) T, (b) q, (c) w_{R}, (d) w_{S}, (e) w_{L}, (f) w_{I} and (g) cloud fraction C, as a function of model level ML for test dataset. See text for explanation of symbols.

mean Jacobians have been calculated from the test dataset. In section 3(b), the accuracy of the Delta-Eddington approximation to radiative transfer will be quantified using a doubling-adding radiative transfer model as a reference. The latter explicitly solves the multiple-scattering effects between adjacent layers and resolves multiple discrete angles of radiance propagation. The second evaluation regarding the forward model deals with the treatment of fractional cloud cover in the plane-parallel model atmospheres that serve as input from, say, NWP models. The oversimplification of subgrid-scale cloud cover variability may lead to the so-called beam-filling effect in the inversion. This effect is also represented in the adjoint of the radiative transfer model so that gradients of the cost function with respect to changes in cloud cover are accounted for. In section 3(c) the linearity of the model is investigated because it determines the applicability of the radiative transfer model as an observation operator in incremental data assimilation systems. This is because these systems rely on the assumption of linearity of the physical processes in the gradient calculations where the increments of control variables to the background state are calculated. The test of the adjoint version of RTTOV-SCATT will not be reproduced here because it is only of relevance for testing the proper technical coding of the adjoint routines once the tangent-linear model has been developed.

(*a*) *Sensitivity*

The analysis of model Jacobians is standard procedure in data assimilation studies because Jacobians provide crucial information on model sensitivity to input perturbations as a function model state. For application in cloud and precipitation radiative transfer the analysis is rather new (Moreau *et al.* 2003; Greenwald *et al.* 2004). The analysis of Jacobians may also provide the baseline for radiometer optimization studies (Lipton 2003; Bauer and Mugnai 2004; Di Michele and Bauer 2006).

Usually, smooth Jacobian structures are preferred for avoiding large discontinuities of increments during the minimization procedures that may cause strong nonlinear response from other physical processes that are active in the analysis scheme. Figure 2 shows mean Jacobians k for each channel with regard to T and q in the presence of precipitation. The q-Jacobians were scaled with a factor of 10 to match the dynamic range of T-Jacobians. Therefore, the k-units are $\Delta K/\Delta K$ and $\Delta K/\Delta$ (kg kg^{-1}), respectively. The Jacobians have been calculated for an ocean surface using the sea surface temperature and near-surface wind speed of the model profiles.

SSMIS channels 1, 2, 3, 4, 5, 6 correspond to Advanced Microwave Sounding Unit (AMSU-A) channels 3, 4, 5, 6, 8, 9 and show a strong sensitivity to T and almost no sensitivity to q. The weighting-function peak altitude increases with increasing channel number so that these channels cover the entire tropospheric temperature distribution. The Jacobians are always positive.

Channel 7 shows both a temperature sensitivity near 50 hPa and a sensitivity to moisture in the upper troposphere which offers an interesting capability for soundings near the tropopause. Channels 8–11 are similar to AMSU-B channels 2–5 and channels 12–18 are similar to Special Sensor Microwave/Imager channels 1–7. They show increased sensitivity to moisture but still rather strong impact from T. With decreasing spectral distance from the absorption line centre at 183.31, the weighting-function peak altitude increases. The sensitivity of all channels to temperature and moisture points at the more difficult task of moisture profile sounding that is always strongly affected by the given temperature profile. The moisture weighting functions are negative if the peak altitude is high and positive if it is near the surface. The latter is a result of the increasing atmospheric absorption with increasing moisture that increases

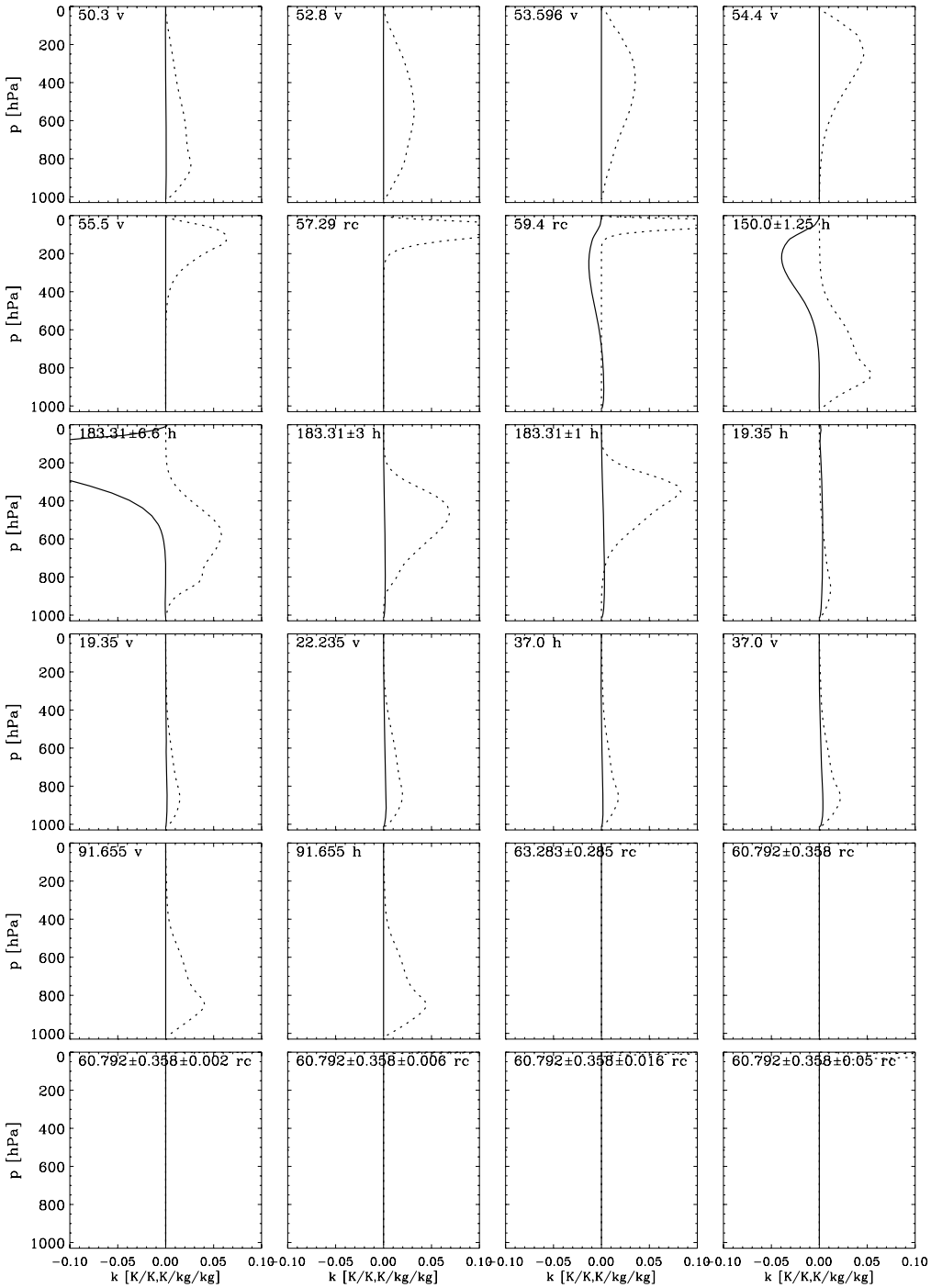

Figure 2. Average Jacobians of temperature T (dotted) and specific humidity q (solid) for all SSMIS channels. Jacobians of q have been multiplied by 10.

the total radiance emission above the radiometrically cold ocean surface. At higher altitudes, the increasing emission of a layer with a given temperature blocks the emission from lower layers with higher temperatures and therefore produces a negative k. Those SSM/I-like channels that provide dual polarization measurements show a slightly larger sensitivity at horizontal polarization due to the lower surface emissivity and therefore larger signal dynamic range.

Figure 3 shows mean Jacobians for cloud liquid water, rain and snow, respectively. The rain Jacobians peak at the top of the rain layer due to increasing attenuation with increasing layer depth. This identifies the general lack of sensitivity to near-surface rainfall intensity that is independent of SSMIS channel. Those sounding channels that have weighting-function peaks in the lower troposphere show sensitivity to precipitation, i.e. channels 1–3. This sensitivity is only weakly inferior to the channels at 19.35 and 22.235 GHz. This, however, depends on the individual profile. It also has to be kept in mind that if sounding channels are used in retrieval schemes, temperature and/or moisture information is required as well to constrain the response to hydrometeor contents. Channels 1–3 show sensitivity to snow as well and their sounding channel character is evident from the reduction of sensitivity to lower-layer contributions with increasing channel number. The general sensitivity to cloud water is as strong as that for rain water. This means that retrieval schemes always have to include both variables to avoid aliasing. The sensitivity to snow is much weaker and mainly apparent at higher window frequencies, i.e. at 91 and 150 GHz. The largest ambiguity between sensitivies to cloud, rain and snow are observed for frequencies at 91 and 150 GHz. These channels show positive k values for cloud water due to absorption effects only, negative sensitivity to snow due to scattering and both positive and negative sensitivity to rain. As for T and q, the horizontally polarized channels show more sensitivity. In all cases, the mesospheric channels do not respond to the presence of parameter variations below 100 hPa.

(*b*) *Forward model*

The primary question in forward-model evaluation is the accuracy of the Delta-Eddington approximation itself. This method basically superimposes isotropic and observation-angle dependent radiance streams of which the latter is determined by the gross shape of the scattering phase function expressed as the asymmetry parameter. Differences between RTTOV-SCATT and a doubling-adding model (Bauer and Schlüssel 1993) have been produced from the test dataset. The doubling-adding model explicitly accounts for multiple radiance streams (here nine between zenith angles $\theta = 0$, 90 degrees) and sequentially calculates the multiple scattering between adjacent layers of variable optical depth.

Figure 4 shows the mean TB differences for all SSMIS channels. The mean difference plots show a slight dependence on observation angle and peak near $\theta = 65$–$70°$. For those channels that show sensitivity to surface emission and reflection this dependence is a function of the change of optical depth and emissivity with angle. For pure sounding channels, it is only a function of the dependence of optical depth on zenith angle. The atmospheric contribution to this effect produces a decrease of the TB differences for zenith angles larger than 70° due to limb darkening that reduces model radiance emission as well as radiance emission differences between models. The average differences are very small and remain well below 0.5–1 K for all channels, in particular where scattering is most effective, i.e. for window channels 8–9, 15–18. The systematic differences for those sounding channels whose weighting functions peak high up in the atmosphere (7, 19–24) are explained by the slightly different treatment of radiance emission from layers with large temperature gradients by both models.

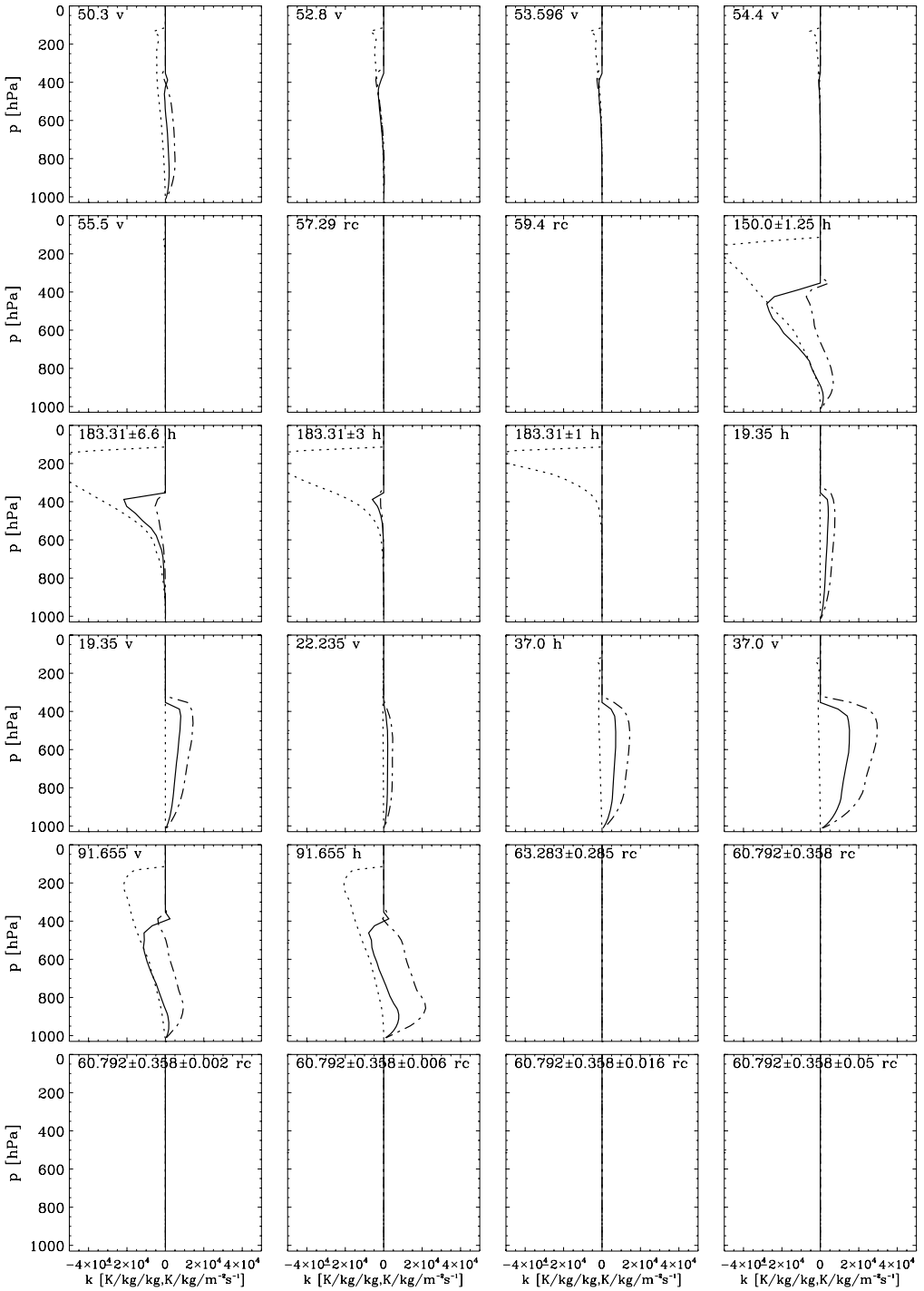

Figure 3. Average Jacobians of w_L (dash-dotted) w_S (dotted) and w_R (solid) for all SSMIS channels. See text for explanation.

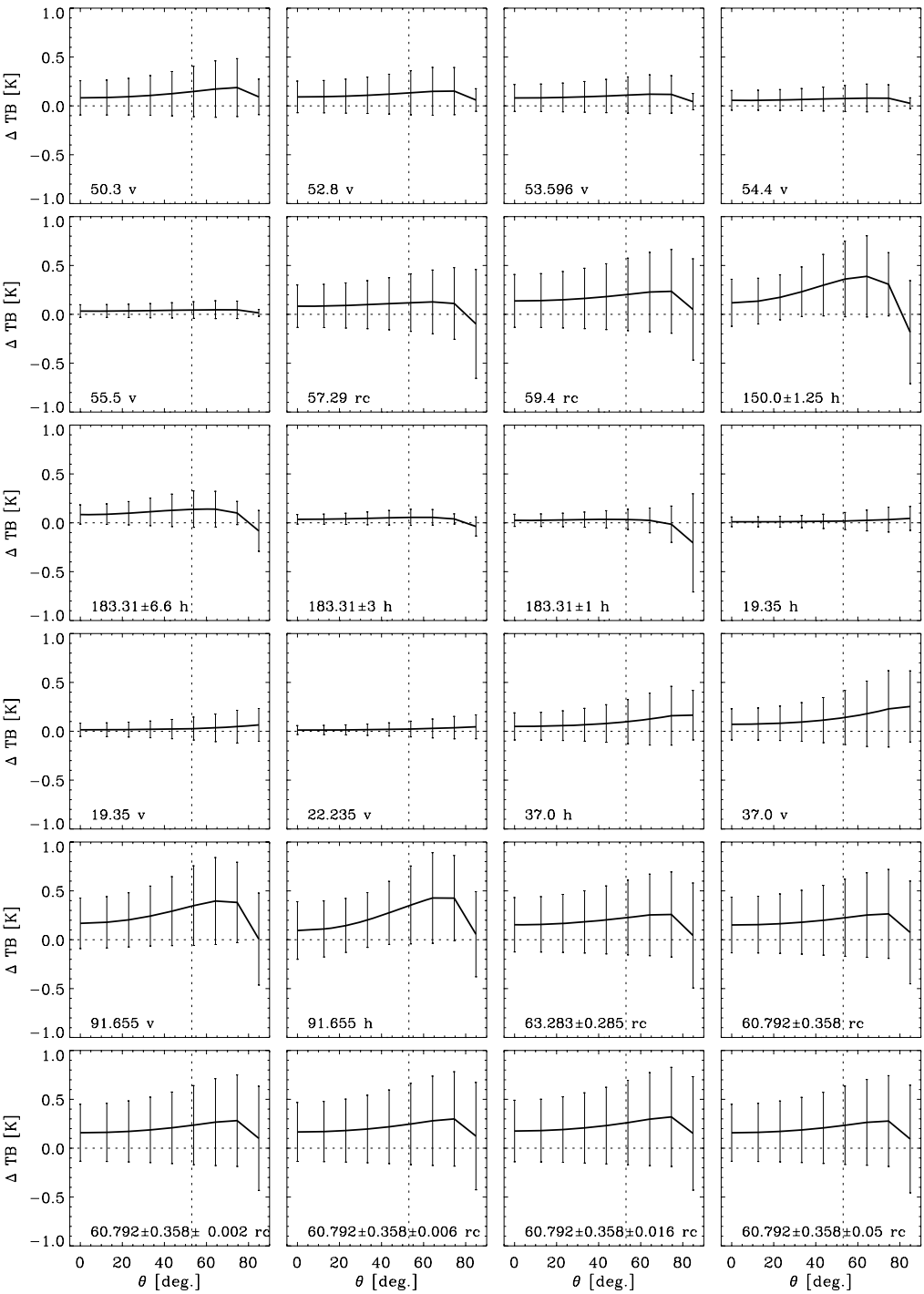

Figure 4. Mean differences in brightness temperature ΔTB and standard deviations between Delta-Eddington and doubling-adding radiative transfer models as a function of zenith angle θ for all SSMIS channels. The vertical line indicates the SSMIS zenith angle at 53.1°.

An increase of uncertainty with frequency in the window channels (8, 12–18) is observed that indicates that the representation of scattering of radiation at particles is one of the main causes. In this study, the doubling-adding model employs the Henyey–Greenstein scattering phase function that predicts angular scattering only from the asymmetry parameter and the scattering angle. The Delta-Eddington model only considers two radiation streams and scales the forward-to-backward scattered radiation in these streams according to the asymmetry parameter. Therefore, the lack of angular resolution and the approximate treatment of multiple scattering within layers explains the model differences. This shortcoming also explains why only for window channels an increase of mean error with increasing zenith angle occurs. An increase of zenith angle also implies an increase in optical depth. Figure 4 shows that the error depends on frequency as well and is thus caused by the stronger scattering along slant paths.

Another radiative transfer modelling issue is the treatment of fractional cloudiness. In the case of one-dimensional (plane-parallel) modelling, the subgrid-scale cloud variability that is an input from the large-scale cloud model must be treated to not systematically underestimate area-averaged rainfall. This is referred to as the beam-filling effect which may account for large systematic errors in both forward and inverse models (e.g. Kummerow 1998). In addition, the error from the neglection of cloud-side emission effects when simulating radiances received by limited aperture microwave antennas may exceed the errors originating from the approximation in the solution of the radiative transfer equation (Roberti *et al.* 1994; Bauer *et al.* 1998). In NWP models, however, the three-dimensional structure of clouds and precipitation are only crudely represented so that a simple approximation to fractional cloud coverage suffices.

RTTOV-SCATT uses the profile of the fractional cloud cover for each layer C as an input parameter. Therefore, the tangent-linear, doubling-adding and k-models also have sensitivity to C. To save computational cost, RTTOV-SCATT applies a two-independent column (2-IC) approach. The maximum C in the profile is retrieved and the hydrometeor contents are scaled with this value. The multiple scattering radiative transfer is applied to the cloud column only and linearly added to the clear-sky contribution, i.e. $\mathrm{TB} = C\mathrm{TB}_{\mathrm{cloud}} + (1 - C)\mathrm{TB}_{\mathrm{clear}}$. Ideally, the IC calculation would involve more columns to better resolve the horizontal variability along the profile. The error of the 2-IC was therefore determined from a comparison with 10-IC and a 100-IC that use 10 or 100 independent columns, respectively. Since the differences between 10-IC and 100-IC were marginal, only the 2-IC vs. 10-IC comparison is reproduced here. It must be noted, however, that the independent column approach, as it is applied here, assumes a maximum overlap of adjacent layers which may not be optimal.

Figure 5 summarizes the mean differences and standard deviations for all SSMIS channels as functions of the maximum C. The results clearly demonstrate a non-negligible bias due to the 2-IC that is strongest where the scattering is strongest and where little atmospheric background absorption occurs. The errors have a maximum at $C = 0.5$ and the maximum values, $\Delta\mathrm{TB}_C$, per channel are listed in Table 1. At $C = 0.5$, the vertical variability of C will reach a maximum so that more columns are required for resolving it. The shape of the biases suggests a simple triangular bias correction, $\Delta\mathrm{TB}$, that may be applied per channel and that only uses the maximum value at $C = 0.5$, and C as a predictor,

$$\Delta\mathrm{TB} = \Delta\mathrm{TB}_C(1 - 2\,|C - 0.5|) \tag{3}$$

that has to be subtracted from the simulated TBs. The result of the bias correction is added in Fig. 5 as dashed lines. Figure 6 shows that in more than 40% of the cases $C = 1$. However, depending on the employed channel, a significant number of profiles

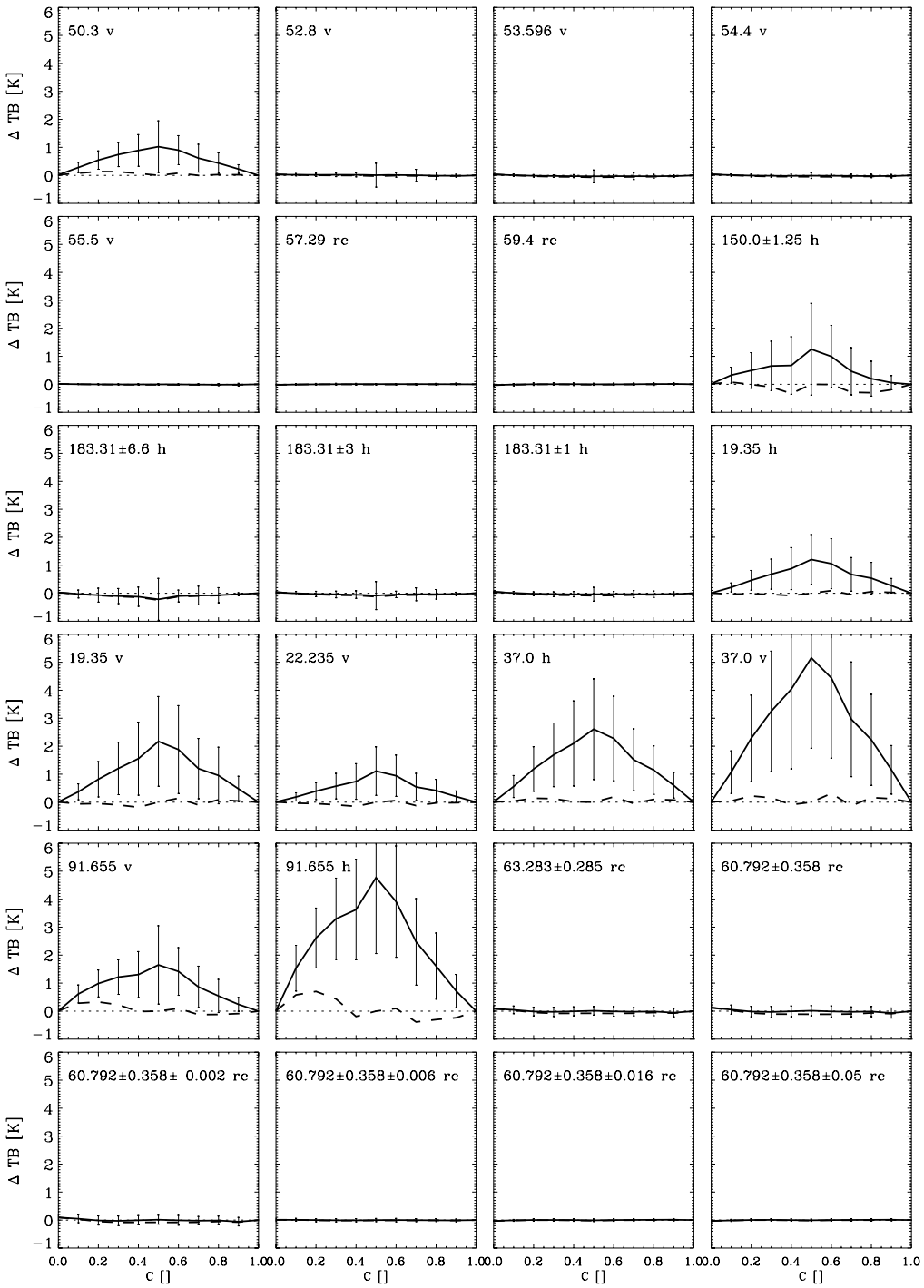

Figure 5. Mean differences in brightness temperature ΔTB (solid) and standard deviations between two-column and ten-column approximations to fractional cloudiness as a function of cloud cover C for all SSMIS channels. Dashed lines show mean differences applying triangular bias correction (for details see text).

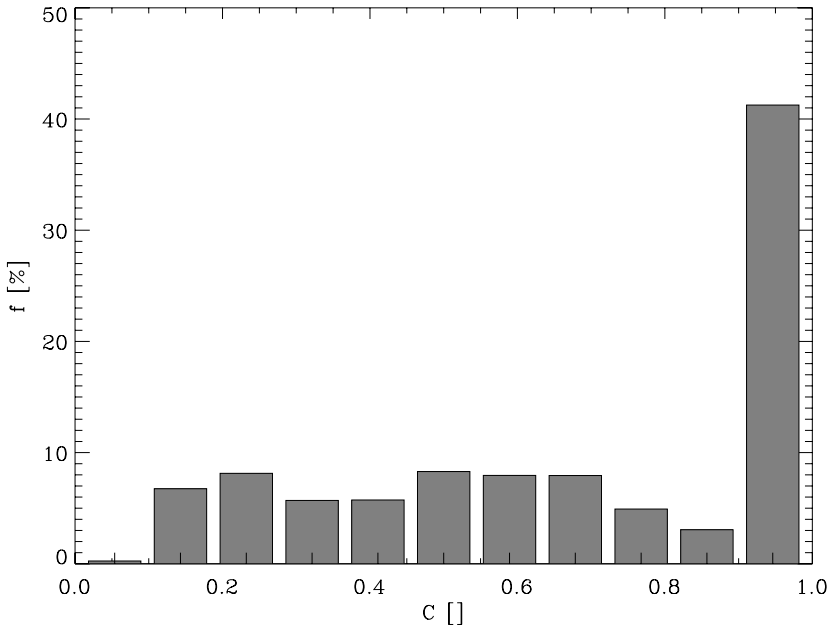

Figure 6. Frequency distribution of fractional cloud cover C.

may produce errors due to the simplification of 2-IC that exceed the radiative transfer errors presented above.

The limited validity of this intercomparison is indicated by the comparison of 2-IC simulations with SSM/I observations (Bauer *et al.* 2006a) that shows smaller biases for the channels between 19.35 and 85.5 GHz. The bias evaluation shown in Fig. 5 therefore largely depends on the assumptions used for the reference model. In our case 10-IC strictly applies the maximum-overlap assumption that assumes that all cloud affected layes are on top of each other. This maximizes the clear-to-cloud fraction in the profile and also produces rainfall in all columns that are cloud affected from the bottom to cloud top. The latter effect may overpredict rain occurrence in case of large fractions of high cloud coverage. This suggests that the differences between 10-IC and 2-IC represent an upper error limit. The possibility of bias correction, however, indicates that some model errors can be corrected in a parametric fashion without loosing computational efficiency through the introduction of more independent columns.

(*c*) *Tangent-linear model*

Ideally, all observation operators have a nearly linear sensitivity to perturbations of the input parameters. Global data assimilation systems mostly employ an incremental formulation of the variational analysis that is based on the assumption that the model responds linearly to perturbations determined from observed minus background fields. The degree of nonlinearity depends on the physical processes that are modelled and their individual as well as comvolved nonlinearity. In the case of scattering radiative transfer, the sensitivity of extinction and scattering is a nonlinear function of hydrometeor content as is the dependence of radiance propagation on layer interaction (multiple scattering). A linearity test can be performed by comparing the output of the tangent-linear model with those from finite difference calculations using the forward model.

For example the ratio

$$F = \frac{H(\mathbf{x} + \lambda\delta\mathbf{x}) - H(\mathbf{x})}{\lambda \mathbf{H}(\delta\mathbf{x})} \tag{4}$$

may be used as a linearity measure in which $\delta\mathbf{x}$ represents the initial perturbation and λ a scaling factor. In the linear case, scaling of the output of the tangent-linear model should produce the same result as the scaling of the input to the forward model. While Bauer *et al.* (2006a) carry out a linear test for a combined moist physics parametrization–radiative transfer observation operator to be used for assimilating microwave radiances in an NWP model analysis system, only the multiple-scattering model is tested here. Note that the perturbations $\delta\mathbf{x}$ apply to hydrometeor contents as well as temperature and humidity so that also those channels are tested that show little sensitivity to clouds and precipitation.

The scaling factor λ usually spans several orders of magnitude to explore a wide range of perturbation sizes. If λ is small, F should converge towards unity with decreasing λ. If λ becomes too small the limited computer accuracy makes F diverge again from unity. In variational analyses, the perturbations are of the order of the uncertainty of the background state. An observation operator (like RTTOV-SCATT) is therefore required to behave rather linearly for perturbations spanning the range between the numerical limitation and the departure of the background state from the observations. Moreover, by scaling the initial perturbations with λ the range of validity of the linearity assumption can be used for defining screening procedures that ensure that the perturbations do not exceed the identified magnitude.

In our case, the analysis $\mathbf{x}_a$ minus first-guess $\mathbf{x}_b$ departures from a 1D-Var analysis (Bauer *et al.* 2006a) serve this purpose. This is because they define the improvement of the first-guess state that was achieved by constraining the retrieval with observations given the defined model and observation errors, respectively. In a 4D-Var direct radiance assimilation, similar first-guess departures can be expected and thus define the dynamic range for which the radiative transfer model should behave linearly. Therefore

$$\delta\mathbf{x} = \mathbf{x}_a - \mathbf{x}_b, \tag{5}$$

which we scale with λ values ranging from 10^{-9} to 1 with increments of 10^1. Figure 7 shows the accumulated results from 8290 precipitation profiles over global oceans. The initial perturbations of rain, snow, cloud water, cloud ice, cloud cover, specific humidity and temperature were taken from the analysis increments of 1D-Var retrievals using SSM/I radiances as observations and ECMWF short-range model forecasts as first-guess estimates.

The results are displayed as qualitative probability distribution functions (pdfs) of $\log_{10}|1 - F|$ in Fig. 7 for all SSMIS channels. The parameter $\log_{10}|1 - F|$ should become smaller with increasing linearity because F will approach 1. At $\log_{10}|1-F| = -1$, the difference between tangent-linear and finite-difference models is 10% and 1% for $\log_{10}|1 - F| = -2$. For larger λ, $\log_{10}|1 - F|$ is expected to increase due to non-linearities as well as for very small λ. The latter is due to the limitations of the numerical accuracy with which ratios of very small numbers can be represented. Ideally, $\log_{10}|1 - F|$ should scale linearly with scaling factor λ. The scaling works best for channels 8–11 that are quite sensitive to water-vapour background absorption and cloud emission at the same time. The window channels, i.e. channels 1–4 and 12–18 show the minimum $\log_{10}|1 - F|$ already for $\log_{10}(\lambda) \approx -4$ while the pure sounding channels, i.e. channels 5–7 and 19–24, have less signal dynamic range and therefore approach numerical accuracy limits for $\log_{10}(\lambda) \approx -3$. The accumulations at $\log_{10}|1 - F| = 0$ are caused by very small initial perturbations that produce zero numerators in F.

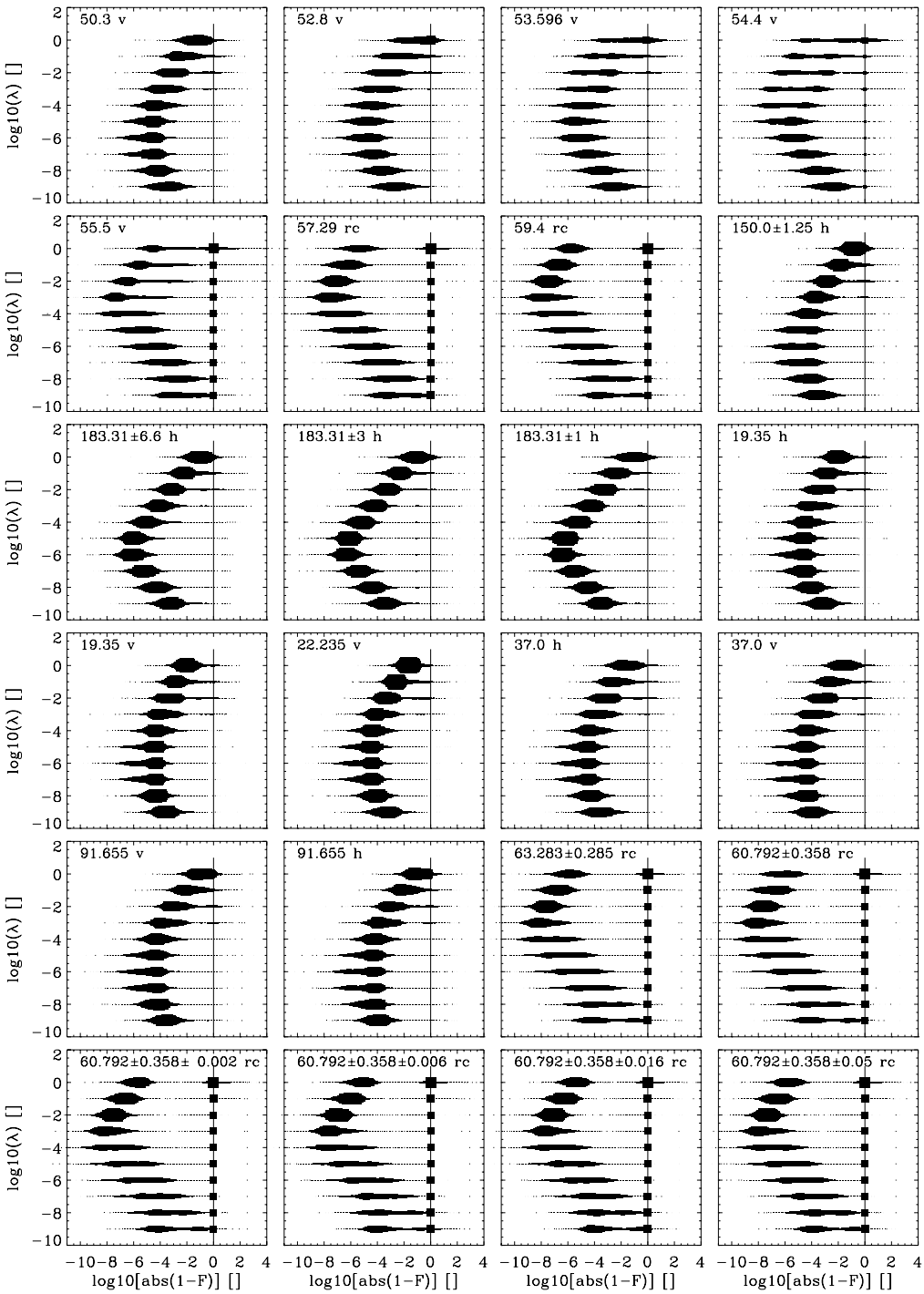

Figure 7. Linearity test parameter $\log_{10}|1-F|$ (see text) as a function of scaling parameter λ from 8290 precipitation profiles for all SSMIS channels. Symbols refer to each λ-scaling and symbols size indicates frequency of occurrence.

The separation of temperature/humidity from cloud/precipitation effects can be observed for channels 2–5. Two different accumulations of $\log_{10}|1-F|$ can be isolated of which the smaller ones belong to the impact of temperature/humidity and the larger ones to cloud/precipitation. Channels 6–7 have little to no sensitivity to hydrometeor perturbations so that only the branch with smaller $\log_{10}|1-F|$ remains.

For a potential direct assimilation of rain affected microwave TBs in an incremental data assimilation system, $\log_{10}|1-F|$ should be as small as possible for $\lambda = 1$ ($\log_{10}(\lambda) = 0$). This requirement is partly fulfilled for a number of channels whose weighting functions peak low enough for being sufficiently sensitive to hydrometeor emission and scattering, namely channel 1 and channels 8–18. All these channels, however, show a small percentage of cases near $\log_{10}|1-F| = 0$ indicating larger nonlinearities which must be identified in a screening procedure prior to the assimilation of the data.

With a proper screening, the most likely candidates for a direct assimilation of microwave radiances in an incremental data assimilation system are channels that show sufficient sensitivity to clouds and precipitation (see Jacobian analysis in Fig. 3) but are less prone to nonlinear response to changes in hydrometeor contents. The first criterion requires channels that are located in spectral window regions. In the case of the SSMIS, these are channels 1–3, 8–10 and 12–18. The second criterion suggests channels 1 and 12–16, potentially also channels 9–10.

4. Discussion

This paper presents a performance analysis of a multiple-scattering radiative transfer model suitable for the assimilation of microwave radiance information in NWP models. The model is part of the NWP-SAF RTTOV model package that is maintained at the Met Office and operationally employed in several NWP centres worldwide. As required for the entire RTTOV model, the scattering component, RTTOV-SCATT, provides forward, tangent-linear, adjoint and Jacobian models. The SSMIS sensor was chosen as a demonstrator instrument in this study because it comprises channels of the three most widely used microwave instruments in NWP at present, namely SSM/I, AMSU-A and AMSU-B. The performance analysis was based on a large profile dataset that was produced within the operational rain assimilation system at ECMWF.

The main results are that the chosen approximation to the solution of the radiative transfer equation is very accurate for the chosen frequency range with errors less than 0.5–1 K. The resulting gain in computational efficiency is substantial so that multiple-scattering radiative transfer calculations are affordable in current global operational analysis systems. A significant error may be produced by the approximation of fractional cloudiness by one cloud/rain and one clear column. This simplification has been chosen to avoid excessive computational cost and may produce maximum biases of 5 K. A simple bias-correction formula was presented which has to be tested on a global scale to verify the significance of this error source. Comparison of modelled with observed SSM/I radiances, however, suggested that the chosen reference mode itself is not optimal because it assumes maximum cloud overlap and the presence of rain between the surface and the highest cloud layer. Future improvements of RTTOV-SCATT will incorporate a more sophisticated treatment of subgrid-scale variability maintaining the computational efficiency.

The assimilation of microwave radiances in an incremental data assimilation framework requires nearly linear model behaviour. The presented analysis suggests that channels at 50.3, 19.35, 22.235, 37.0 GHz, and potentially 183.31 ± 3 and 183.31 ± 7 GHz,

show sufficient linearity in the given model context. However, prior to assimilation a screening of those situations is required for which linearity is not assured because for all channels a small but non-negligible number of cases with nonlinear dependence of radiances on input parameter perturbations was observed.

In nonlinear variational assimilation systems (e.g. Vukićević *et al.* 2004; Zupanski *et al.* 2005) the deviations from linearity that were shown in this study are less of a concern. However, depending on the model's sensitivity patterns and the case-dependent nonlinearities, convergence problems and discontinuous cost-function developments during minimization may occur even in slightly nonlinear situations. In general, the combination of the smoothness of the sensitivity of microwave radiances to changes in temperature, moisture, and hydrometeor contents and the not too nonlinear behaviour exhibited by RTTOV-SCATT suggest its usefulness in most variational assimilation systems.

With future versions of RTTOV, the model will be further developed to account for more sensors and to reduce potential sources of uncertainties. Most obvious candidates for improvement are the treatment of subgrid-scale cloud variability and better parametrizations of particle single-scattering properties. The former mainly requires a better specification of the 'effective' cloudiness for a given profile since it is not feasible to perform radiative transfer calculations for more than 2–3 independent columns inside a data assimilation system. The effective cloudiness must be a compromise between minimizing radiative transfer errors and ensuring physical consistency with the true cloud-cover profile. The largest impact on the improvement of particle single-scattering calculations can be expected from better particle size distribution models because these mainly determine the absorption-to-scattering ratio per liquid-water unit. All potential upgrades, however, must be applicable to the wide range of natural variability unless additional information from independent observations can be obtained for constraining the choice of a particular model.

Acknowledgements

The authors are very grateful to Dr Andrew Collard for the implementation of the k-routines and two anonymous reviewers for valuable suggestions that greatly helped to improve the paper.

Appendix A

RTTOV-SCATT

The radiative transfer equation can be expressed as the differential change of radiance L at frequency ν along the propagation path (here the vertical path z and zenith angle $\mu = \cos\theta$) through the atmosphere:

$$\mu \frac{\mathrm{d}L(z;\,\mu)}{k_{\mathrm{ext}}\,\mathrm{d}z} = L(z;\,\mu) - J(z;\,\mu). \tag{A.1}$$

The volume extinction coefficient k_{ext} is composed of scattering k_{sct} and absorption k_{abs} contributions, i.e. $k_{\mathrm{ext}} = k_{\mathrm{sct}} + k_{\mathrm{abs}}$; z denotes altitude and J is the source term that covers contributions from scattering (hydrometeors) and emission (at microwaves: oxygen, water vapour, dry air, hydrometeors):

$$J(z;\,\mu) = \frac{\omega_0}{2} \int_{-1}^{1} L(z;\,\mu')P(\mu;\,\mu')\,\mathrm{d}\mu' + (1-\omega_0)B\{T(z)\}, \tag{A.2}$$

where $\omega_0 = k_{\mathrm{sct}}/k_{\mathrm{ext}}$ denotes the single-scattering albedo and provides a measure for the fraction of scattered radiation, while $1 - \omega_0$ is the fraction of absorbed radiation. $B\{T(z)\}$ is the black-body equivalent radiance according to temperature T at level z. Scattering of radiance is expressed in terms of a normalized scattering phase function:

$$\int_{-1}^{1} P(\mu;\, \mu')\, \mathrm{d}\mu' = 1, \tag{A.3}$$

describing the distribution of incident radiance (μ') to observation direction (μ).

In Eqs. (A.1)–(A.3), the azimuth angle dependence of radiance propagation has been neglected. This is acceptable at microwaves because no direct radiation source exists and the diffuse radiation field only shows a dependence in azimuthal direction if this is introduced by non-spherical particle scattering or reflection of radiation at the surface. However, the current implementation of RTTOV does not resolve the azimuth angle so that this dependency is omitted here.

The solution of Eq. (A.1) is only numerically possible if approximations to J are applied that account for its dependence on layer interaction. The Eddington approximation (e.g. Kummerow 1993) to radiative transfer represents an example for an approximative method. The approximation lies in the development of the radiance vector and phase function to the first order so that only one angle (i.e. the observation angle) is needed and the anisotropic radiance field is decomposed into an isotropic and anisotropic component, respectively:

$$\left.\begin{aligned} L(z,\, \mu) &= L_0(z) + \mu\, L_1(z), \\ P(\cos\Theta) &= 1 + 3g\cos\Theta, \end{aligned}\right\} \tag{A.4}$$

with local and azimuth-independent scattering angle $\cos\Theta = \pm\mu\mu'$ and asymmetry parameter g representing the angular mean of the scattering phase function. Then, the source function translates to

$$J(z,\, \mu) = \{1 - \omega_0(z)\}B\{T(z)\} + \omega_0(z)\{L_0(z) + g(z)\mu L_1(z)\} \tag{A.5}$$

for azimuthally averaged fields.

Two mixed equations can be obtained by inserting Eqs. (A.5) and (A.4) into Eq. (A.1):

$$\left.\begin{aligned} \frac{\mathrm{d}L_0(z)}{\mathrm{d}z} &= -k(z)\{1 - \omega_0(z)g(z)\}L_1(z), \\ \frac{\mathrm{d}L_1(z)}{\mathrm{d}z} &= -3k(z)\{1 - \omega_0(z)\}[L_0(z) - B\{T(z)\}]. \end{aligned}\right\} \tag{A6}$$

If z' is the height within a layer and assuming that k, g and ω_0 do not vary with an individual layer, their derivatives with respect to z' can be neglected and the second derivative of, for example, L_0 provides

$$\frac{\mathrm{d}^2 L_0(z)}{\mathrm{d}z^2} = \Lambda^2(z)[L_0(z) - B\{T(z)\}], \tag{A.7}$$

$$\Lambda^2(z) = 3k^2(z)\{1 - \omega_0(z)\}\{1 - \omega_0(z)g(z)\}. \tag{A.8}$$

For an individual atmospheric layer, the general solution is

$$L_0(z) = D^+ \exp(\Lambda z) + D^- \exp(-\Lambda z) + B(T_0) + B_1 \Delta z. \tag{A.9}$$

A linear dependence of temperature with optical depth is assumed in the layer, i.e. $B(T) = B(T_0) + B_1 \Delta z$ with lapse rate B_1, temperature at the bottom layer limit T_0 and layer depth Δz.

The coefficients $D^{\pm}$ have to be computed for all layers from the respective boundary conditions, i.e. space background radiation at the top of the atmosphere ($z = z^*$), polarized (p) surface emission and reflection at the bottom of the atmosphere ($z = z_0 = 0$) as well as from the requirement of flux continuity at the layer interfaces:

$$\left.\begin{aligned} \left(L_0 - \frac{\partial L_0}{h \partial z}\right)_{z=z^*} &= B(2.7), \\ \left(L_0 + \frac{\partial L_0}{h \partial z}\right)_{z=0} &= \overline{\epsilon}_p B(T) + (1 - \overline{\epsilon}_p)\left(L_0 - \frac{\partial L_0}{h \partial z}\right)_{z=0}, \\ \left(L_0 \pm \frac{\partial L_0}{h \partial z}\right)^{i}_{z=z_i} &= \left(L_0 \mp \frac{\partial L_0}{h \partial z}\right)^{i+1}_{z=z_i}. \end{aligned}\right\} \tag{A.10}$$

The terms in brackets denote the downward (−) and upward (+) directed flux densities, $h = 1.5\, k(1 - \omega_0 g)$; $z = z_i$ denotes the ith layer interface between ith and $(i + 1)$th layer. Since the continuity requirement applies to flux densities, the polarized hemispheric emissivity ϵ_p is used which is calculated from the integration of the specular emissivity over the hemisphere:

$$\overline{\epsilon}_p = 2 \int_0^1 \epsilon_p(\mu) \mu \, \mathrm{d}\mu. \tag{A.11}$$

Usually, the integration in Eq. (A.11) is carried out per channel and profile by summation over a limited number of M discrete Gaussian quadrature angles μ_j, using specular emissivities $\epsilon_{p,j}$:

$$\overline{\epsilon}_p = 2 \sum_{j=1}^{M} \epsilon_{p,j}(\mu_j) w_j \mu_j, \tag{A.12}$$

with quadrature weighting coefficient w_j for polarization p. In RTTOV-SCATT, $\overline{\epsilon}_p$ is represented by the 'effective' emissivity formulation developed by Deblonde and English (2001) so that no integration is required.

A system of linear equations of the form $A\, D^{\pm} = B$ can be formulated from inserting Eq. (A.9) into Eqs. (A.10). For N atmospheric layers, this system contains $2\,(N - 2)$ equations for the layer interfaces as well as one at the top and bottom of the atmosphere, respectively. Therefore, A is a $2N \times 2N$ matrix and B is a $2N$ vector with elements a_{mn} and b_m, respectively. For each layer, i, $j = 2i$,

$$\left.\begin{aligned} a_{j,j-1} &= L_i^{+} \exp(\Lambda_i \Delta z_i), \\ a_{j,j} &= L_i^{-} \exp(-\Lambda_i \Delta z_i), \\ a_{j,j+1} &= -L_i^{+}, \\ a_{j,j+2} &= -L_i^{-}, \\ b_j &= C_j - C_i, \end{aligned}\right\} \tag{A.13}$$

$$\left.\begin{aligned} a_{j+1,j-1} &= L_i^- \exp(\Lambda_i \Delta z_i), \\ a_{j+1,j} &= L_i^+ \exp(-\Lambda_i \Delta z_i), \\ a_{j+1,j+1} &= -L_i^-, \\ a_{j+1,j+2} &= -L_i^+, \\ b_{j+1} &= C_i - C_j, \end{aligned}\right\} \tag{A.14}$$

and for the top and bottom layers:

$$\left.\begin{aligned} a_{1,1} &= L_1^- - \overline{\rho}_p L_1^+, \\ a_{1,2} &= L_1^+ - \overline{\rho}_p L_1^-, \\ b_1 &= B(T_\mathrm{s})(\overline{\epsilon}_p + \overline{\rho}_p - 1) + C_1(\overline{\rho}_p + 1), \end{aligned}\right\} \tag{A.15}$$

$$\left.\begin{aligned} a_{2N,2N-1} &= L_N^+ \exp(\Lambda_N \Delta z_N), \\ a_{2N,2N} &= L_N^- \exp(-\Lambda_N \Delta z_N), \\ b_{2N} &= B(T_\mathrm{sp}) - B(T_{N-1}) - C_N, \end{aligned}\right\} \tag{A.16}$$

with $C_i = B_{1,i}/h_i$, $L_i^\pm = 1 \pm \Lambda_i/h_i$, $\overline{\rho}_p = 1 - \overline{\epsilon}_p$, and $h_i = 1.5\, k_i(1 - \omega_{0,i} g_i)$; $B(T_\mathrm{s})$ denotes radiance emitted by the surface with skin temperature T_s, $B(T_\mathrm{sp})$ corresponds to space radiation (here 2.7 K), $B_{1,i}$ is the ith layer's lapse rate and $B(T_{n-1})$ the radiance according to temperature at the interface between layers N and $N-1$.

The number of vertical layers follows the operational model layer definition at ECMWF. In the version that was used for this study, the model atmosphere consists of $N = 60$ layers between surface and 0.1 hPa. For deep tropical convection, clouds may occur in the lower 40 levels and liquid-water and ice clouds as well as liquid and frozen precipitation co-exist above freezing level according to the model's formulation of particle freezing.

The source term from Eq. (A.5) has to be integrated for each layer between $z' = 0$ and $z' = \Delta z_i$. This is performed for up-/downwelling radiances, respectively:

$$\left.\begin{aligned} J_i^+ &= J_{a,i}^+ \alpha_i + J_{b,i}^+ \beta_i + J_{c,i}^+ \gamma_i + J_{d,i}^+ \delta_i, \\ J_i^- &= J_{a,i}^- \alpha_i + J_{b,i}^- \beta_i + J_{c,i}^- \gamma_i + J_{d,i}^- \delta_i, \end{aligned}\right\} \tag{A.17}$$

with

$$\left.\begin{aligned} \alpha_i &= B_{0,i} - \frac{3 g_i \omega_{0,i} \mu B_{1,i}}{2 h_i}, \\ \beta_i &= B_{1,i}, \\ \gamma_i &= D_i^+ \omega_{0,i} \left(1 - \frac{g_i \mu \Lambda_i}{2 h_i}\right), \\ \delta_i &= D_i^- \omega_{0,i} \left(1 + \frac{g_i \mu \Lambda_i}{2 h_i}\right), \end{aligned}\right\} \tag{A.18}$$

and partial source terms

$$\left.\begin{aligned} J^+_{a,i} &= 1 - \tau_i, \\ J^+_{b,i} &= \Delta z_i - \frac{\mu(1-\tau_i)}{k_i}, \\ J^+_{c,i} &= \frac{k_i}{k_i + \Lambda_i \mu}\{\exp(\Delta z_i \Lambda_i) - \tau_i\}, \\ J^+_{d,i} &= \frac{k_i}{k_i - \Lambda_i \mu}\{\exp(-\Delta z_i \Lambda_i) - \tau_i\}, \end{aligned}\right\} \tag{A.19}$$

$$\left.\begin{aligned} J^-_{a,i} &= 1 - \tau_i, \\ J^-_{b,i} &= \frac{\mu}{k_i}(1-\tau_i) - \tau_i \Delta z_i, \\ J^-_{c,i} &= \frac{k_i}{\Lambda_i \mu - k_i}[\exp\{\Delta z_i(\Lambda_i - k_i/\mu)\} - 1], \\ J^-_{d,i} &= \frac{k_i}{\Lambda_i \mu + k_i}[1 - \exp\{-\Delta z_i(k_i + \Lambda_i \mu)/\mu\}]. \end{aligned}\right\} \tag{A.20}$$

Radiance $B_{0,i}$ corresponds to the temperature at the bottom interface of layer i. Finally, the integration of contributions from each layer through the atmosphere is carried out, first downward then upward:

$$\left.\begin{aligned} L^-_i &= L^-_{i+1}\tau_i + J^-_i, \\ L^+_i &= L^+_{i-1}\tau_i + J^+_i, \end{aligned}\right\} \tag{A.21}$$

with

$$\left.\begin{aligned} L^-_{N+1} &= B(2.7), \\ L^+_0 &= B(T_s)\epsilon_p + (1-\epsilon_p)L^-_1. \end{aligned}\right\} \tag{A.22}$$

As ϵ_p is the polarized surface emissivity, $L_0 \uparrow$ has to be calculated for each polarization.

The background (i.e. clear-sky) absorption contribution as well as surface reflection and emission are calculated with the corresponding clear-sky RTTOV routines. The optical properties of hydrometeors are stored in satellite sensor-specific coefficient files. Particle single scattering was calculated applying Mie-theory to spherical particles composed of water for cloud water and rain and air–ice mixtures for ice and frozen precipitation. The dieletric properties for frozen particles were combined following Maxwell–Garnett's formulation assuming ice as the matrix and air as the inclusion material. Cloud water and ice particles follow modified Gamma size distributions while liquid and frozen precipitation size distribution were assumed to have an onential shape with fixed offsets and liquid-water content-dependent slopes. More details of the underlying assumptions on particle permittivity as a function of frequency and temperature, size distribution as a function of hydrometeor type and water/ice content, particle density as a function of hydrometeor type as well as the relevant references can be found in Bauer (2001).

The Delta-scaling (Joseph *et al.* 1976) modifies k_i, $\omega_{0,i}$, and g_i as a consequence of the approximation of the fractional forward peak of the phase function by a delta-function:

$$g'_i = \frac{g_i}{1+g_i}, \quad \omega'_{0,i} = \frac{(1-g_i)^2\omega_{0,i}}{1-g^2\omega_{0,i}}, \quad k'_i = (1-\omega_{0,i}g_i^2)k_i, \tag{A.23}$$

which has proved to significantly improve the treatment of radiative transfer in two-stream-type models in strongly scattering media. Therefore, k'_i, $\omega'_{0,i}$, and g'_i replace k_i, $\omega_{0,i}$, and g_i where required in all the above equations. The optical quantities k'_i, $\omega'_{0,i}$, g'_i, h_i, and Λ_i are calculated per layer, per frequency and per profile.

References

Bauer, P. 2001 Including a melting layer in microwave radiative transfer simulation for clouds. *Atmos. Res.*, **57,** 9–30

Bauer, P. and Mugnai, A. 2004 Precipitation profile retrievals using temperature–sounding microwave observations. *J. Geophys. Res.*, **108**(D23)**,** 4730, doi: 10.1029/2003JD003572

Bauer, P. and Schlüssel, P. 1993 Rainfall, total water, ice water and water-vapour over sea from polarized microwave simulations and SSM/I data. *J. Geophys. Res.*, **98,** 20737–20759

Bauer, P., Schanz, L. and Roberti, L. 1998 Correction of three–dimensional effects for passive microwave retrievals of convective precipitation. *J. Appl. Meteorol.*, **37,** 1619–1632

Bauer, P., Lopez, P., Benedetti, A., Salmond, D. and Moreau, E. 2006a Implementation of 1D+4D-Var Assimilation of Precipitation Affected Microwave Radiances at ECMWF. Part I: 1D-Var. *Q. J. R. Meteorol. Soc.* (in press)

Bauer, P., Lopez, P., Benedetti, A., Salmond, D., Saarinen, S. and Bonazzola, M. 2006b Implementation of 1D+4D-Var Assimilation of Precipitation Affected Microwave Radiances at ECMWF. Part II: 4D-Var. *Q. J. R. Meteorol. Soc.* (in press)

Chevallier, F. and Bauer, P. 2003 Model rain and clouds over oceans: Comparison with SSM/I observations. *Mon. Weather Rev.*, **131,** 1240–1255

Chevallier, F., Bauer, P., Mahfouf, J.-F. and Morcrette, J.-J. 2002 Variational retrieval of cloud profile from ATOVS observations. *Q. J. R. Meteorol. Soc.*, **128,** 2511–2525

Deblonde, G. and English, S. 2001 'Evaluation of the FASTEM-2 fast microwave oceanic surface emissivity model'. Pp. 67–78 in *Tech. Proc. ITSC-XI*, Budapest 20–26 Sept. 2000,

Di Michele, S. and Bauer, P. 2006 Pasive microwave radiometer channel selection based on cloud and precipitation information content. *Q. J. R. Meteorol. Soc.* (in press)

Eyre, J. R. 1991 A fast radiative transfer model for satellite sounding systems. ECMWF Tech. Memo. No. 176. European Centre for Medium-Range Weather Forecasts, Shinfield Park, Reading, Berkshire RG2 9AX, UK

Greenwald, T. J., Hertenstein, R. and Vukićević, T. 2002 An all-weather observational operator for radiance data assimilation with mesoscale forecast models. *Mon. Weather Rev.*, **130,** 1882–1897

Greenwald, T. J., Vukićević, T., Grasso, L. D. and Vonder Haar, T. 2004 Adjoint sensitivity analysis of an observational operator for visible and infrared cloudy-sky radiance assimilation. *Q. J. R. Meteorol. Soc.*, **130,** 685–705

Ide, K., Courtier, P., Ghil, M. and Lorenc, A. 1997 Unified notation for data assimilation: Operational, sequential and variational. *J. Meteorol. Soc. Jpn.*, **75,** 181–189

Joseph, J. H., Wiscombe, W. J. and Weinman, J. A. 1976 The Delta-Eddington approximation for radiative flux transfer. *J. Atmos. Sci.*, **33,** 2452–2459

Kummerow, C. 1993 On the accuracy of the Eddington approximation for radiative transfer in the microwave frequencies. *J. Geophys. Res.*, **98**(D2)**,** 2757–2765

1998 Beamfilling errors in passive microwave rainfall retrievals. *J. Appl. Meteorol.*, **37**(D2)**,** 356–370

Lipton, A. 2003 Satellite sounding channel optimization in the microwave spectrum. *IEEE Trans. Geosci. Remote Sens.*, **41**(D2)**,** 761–781

Moreau, E., Bauer, P. and Chevallier, F. 2003 Variational retrieval of rain profiles from spaceborne passive microwave radiance observations. *J. Geophys. Res.*, **108**(D16)**,** 4521, doi: 10.1029/2002JD003315

Roberti, L., Haferman, J. and Kummerow, C. 1994 Microwave radiative transfer through horizontally inhomogeneous precipitating clouds. *J. Geophys. Res.*, **99**(D8)**,** 16707–16718

Saunders, R., Brunel, P., English, S. J., Bauer, P., O'Keeffe, U., Francis, P. and Rayer, P. 2005 RTTOV-8 Science and validation report. NWP SAF Report, NWPSAF-MO-TV-007

Smith, E., Bauer, P., Marzano, F. S., Kummerow, C. D., McKague, D., Mugnai, A. and Panegrossi, G. 2002 Intercomparison of microwave radiative transfer models for precipitating clouds. *IEEE Trans. Geosci. Remote Sens.*, **40,** 541–549

Swadley, S. D. and Chandler, J. 1992 'The Defense Meteorological Program's Special Sensor Microwave Imager/Sounder (SSMIS): Hardware and retrieval algorithms'. Pp. 457–461 in Preprints of sixth conference on satellite meteorology and oceanography, 5–10 January 1992, Atlanta, GA. American Meteorological Society

Vukićević, T., Greenwald, T., Zupanksi, M., Zupanksi, D., Vonder Haar, T. and Jones, A. S. 2004 Mesoscale cloud state estimation from visible and infrared satellite radiances. *Mon. Weather Rev.*, **132,** 3066–3077

Weinman, J. A. and Davies, R. 1978 Thermal microwave radiances from horizontally finite clouds of hydrometeors. *J. Geophys. Res.*, **83**(C6)**,** 3099–3107

Zupanski, M., Zupanski, D., Vukićević, T., Eis, K. and Vonder Haar, T. 2005 CIRA/CSU four-dimensional variational data assimilation system. *Mon. Weather Rev.*, **133,** 829–843